# Microbial gas-sensing property of *Escherichia coli* with mixed metal catalyst $MgFe_2O_4$

**Sachin Bangale[1,*], Vinay Chaugule[3], Reshma Prakshale[1] and Sambaji Bamane[2]**

[1]Gopinath Mahadev Vedak College of Science, Tala-Raigad 402 111, India
[2]Metal Oxide Research Laboratory, Department of Chemistry, Dr Patangrao Kadam Mahavidyalaya, Sangli 416 416, India
[3]Department of Microbiology, Miraj Mahavidyalaya Miraj, Sangli 416 410, India

**A thick biofilm of *Escherichia coli* was applied to a mixed metal catalyst, $MgFe_2O_4$ synthesized using solution combustion technique. The isolated pure culture of *E. coli* was mixed with the prepared mixed metal catalyst. Both preparation processes were convenient, environment-friendly and efficient. The $MgFe_2O_4$ materials were characterized by TG/DTA and XRD. The prepared thick biofilm of *E. coli* with $MgFe_2O_4$ was measured by exposing to different reducing gases. It was found that *E. coli* acted as a sensor and showed various responses to different gases at various operating temperatures with metal catalyst. The prepared biofilm sensor exhibited fast response and good recovery at low concentration.**

**Keywords:** Biofilm, *Escherichia coli*, gas sensors, mixed metal catalyst.

*ESCHERICHIA COLI* is a Gram-negative, rod-shaped bacterium commonly found in warm-blooded animals. Most *E. coli* strains are harmless, but there are opportunistic pathogens too and these are easy to isolate. The genetic map of *E. coli* is well known; the first complete DNA sequence of an *E. coli* genome (laboratory strain K-12 derivative MG1655) was published in 1997. It was found to be a circular DNA molecule 4.6 million base pairs in length, containing 4288 annotated protein-coding genes (organized into 2584 operons), seven ribosomal RNA (rRNA) operons and 86 transfer RNA (tRNA) genes. Despite having been the subject of intensive genetic analysis for approximately 40 years, a large number of these genes were previously unknown. The coding density was found to be very high, with a mean distance between genes of only 118 base pairs[1]. *E. coli* helps the body break down and digest the food. The bacteria are motile with peritrichous flagella and easily isolated on synthetic and semi-synthetic media. The generation time of *E. coli* is 20 min. The size of the bacteria is about 0.2 μm. Due to its small size, *E. coli* has been used in the present study along with nanocrystalline magnesium ferrite ($MgFe_2O_4$; grain size 15–35 μm) as a catalyst.

*For correspondence. (e-mail: bangale_sv@rediffmail.com)

Spinel of the type attract research interest because of their versatile practical applications[2,3]. Spinel ferrites with the general formula $AFe_2O_4$ (A = Mn, Co, Ni, Mg or Zn) are important magnetic materials because of their interesting magnetic and electrical properties with chemical and thermal stabilities[4]. $MgFe_2O_4$ has a cubic structure of normal spinel-type and is a soft magnetic *n*-type semiconducting material, which finds a number of applications in heterogeneous catalysis, adsorption, sensors and in magnetic technologies[5,6]. Recently, nanostructures of magnetic materials have received more attention because of their novel properties, that are significantly different from those of their bulk counterparts[7–10]. There is now increased interest in the study of gas-sensing properties of ferrites[11]. $MgFe_2O_4$ is among the important ferrites with spinel structure[12–14]. It is used as catalyst[15] and acts as a good humidity sensor[16]. It is also an *n*-type semiconductor with the band gap of 2.18 V (ref. 17).

At present, there is greater need for a novel gas sensor capable of providing reliable operation in harsh environments. Such sensors find a range of applications, including monitoring of traffic pollutants or food quality with specially designed electronic noses[18,19]. Gas sensors based on metal oxides are commonly used in the monitoring of toxic pollutants and can provide the necessary sensitivity, selectivity and stability required by such a system[20]. Commonly used oxides include zinc oxide, titanium dioxide, iron oxide, tungsten oxide and tin oxide. These materials have been successfully employed to detect a range of gas vapours, particularly ethanol, methanol and propanol[21,22].

Ferrites serve as a good class of sensing materials, but they suffer from the drawback of being at higher temperature 300–400°C (ref. 23). Consequently, it is interesting to study the gas-sensing properties of $MgFe_2O_4$. The gas-sensing efficiency of a material depends on its microstructural properties, which are related to its method of preparation. $MgFe_2O_4$ is routinely synthesized by combustion method of precursors zinc nitrate, magnesium nitrate and glycine as fuel[24]. Some wet methods, including co-precipitation[25], sol–gel[26], microemulsions[27], oxidation techniques[28] and hydrothermal synthesis[29] have been employed for preparation of oxide. An ideal process should be simple and environmental-friendly. A novel preparation technique of nanomaterial combustion synthesis at ambient conditions has been developed to prepared nanosized compounds. It is a high-yielding, low-cost and facile synthesis method.

In this study, a powder of nanoparticles *E. coli* was prepared and mixed with $MgFe_2O_4$ nanoparticles. The latter were synthesized by novel combustion reaction. One of our aims is to develop a general synthesis method and explore the gas-sensing properties of *E. coli* with catalyst $MgFe_2O_4$, which acts as nanopowder. Furthermore, *E. coli* with catalyst $MgFe_2O_4$ biofilm acts as gas sensor and shows excellent gas-sensing responses to vari-

ous reducing gases. We found the process to be convenient, environment-friendly, inexpensive and efficient. The gas sensing measurements were carried out by the home-made gas detecting system at room temperature. The ultimate objective of this study is to explore the possibility of application of the $MgFe_2O_4$ biofilm in detecting ammonia gas.

Sewage is the raw material source for *E. coli*. One loop-full sample from the sewage was streaked sterilized MacConkey agar plate. The plate was incubated at 37°C for 24 h. The pink-coloured colonies were selected for confirmation of *E. coli* using IMViC test. A single isolated colony showed positive results for indol and methyl red tests, but negative for V.P. and citrate utilization tests, thus confirming the presence of *E. coli*.

The confirmed colony was streaked on another sterilized MacConkey agar plate for enrichment purpose. All plates were incubated at 37°C for 24 h. After incubation, septically scrub the growth of *E. coli* in distilled water. It was then centrifuged to get pellets of *E. coli*. The pellets were allowed to dry to form a powder, which was directly used for further studies.

In this study nanocrystalline $MgFe_2O_4$ powder was prepared using combustion technique. The applied precursor materials were magnesium nitrate hexahydrate, $Mg(NO_3)_2{\cdot}6H_2O$, iron nitrate hexahydrate, $Fe(NO_3)_2{\cdot}6H_2O$ and glycine with high purity in 99.9%, 98% and 99.9% respectively (all materials were purchased from AR Grade from company Aldrich). Glycine has high heat combustion property. Hence it is generally used as organic fuel, providing a good platform for redox reactions during the course of combustion. Initially, magnesium nitrate, iron nitrate and glycine were taken in the proportion 1 : 1 : 4, and dissolved in a beaker while stirring slowly using a glass rod till a clear solution was obtained. The prepared solution was evaporated on a hot plate in the temperature range 70–80°C resulting in the formation of a thick gel. The gel was kept on a hot plate for auto-combustion and was heated in the temperature range 170–180°C. The nanocrystalline $MgFe_2O_4$ powder was formed within a few minutes. It was sintered at 500°C, 600°C, 700°C and 800°C for about 4 h till it gives a brown-coloured, shiny powder of nanocrystalline $MgFe_2O_4$ (ref. 30).

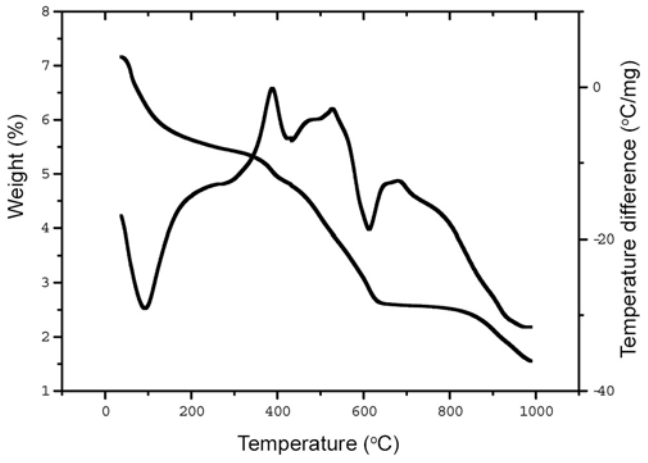


**Figure 1.** Thermo gravimetric differential analysis curve of mixed precursor $MgFe_2O_4$.

The prepared samples were characterized using TG/DTA thermal analyser (SDT Q600 V 20.9 Build 20). The crystalline structures of the powder were analysed with XRD Philips Analytic X-ray B.V. PW-3710 based model diffraction analysis using Cu-$K_\alpha$ radiation with a wavelength 1.5418 Å, scanning electron microscope (JEOL JED 2300), transmission electron microscope operating at 200 kV. Thickness measurements were carried out using a Taylor–Hobson (Talystep, UK) system. Thermoelectric power measurements (TEP) were carried out in the laboratory. Electrical and gas sensing properties were measured using a static gas sensing system.

The paste of *E. coli* and nanocrystalline $MgFe_2O_4$ was screen-printed on a glass substrate in desired patterns. The film prepared was fired at 37°C for 4 h. Silver contact was made by vacuum evaporation and the electrical property was measured. Thickness of the prepared film was 0.70–0.8 μm.

The performance of the sensors was examined using a static gas-sensing system. The electrical feeds were applied through the base plate. The heating wire was fixed on the base plate to heat the sample under required operating temperatures. The current passing through the heating element was monitored in triplicate form using relay with adjustable ON and OFF and at each time interval. Cr–Al thermocouple was used to sense the operating temperature of the sensors. The output of the thermocouple was connected to digital temperature indicators. Gas inlet valve was fitted at one port of the base plate. The required gas concentration inside the static system was achieved by injecting a known volume of test gas using a gas-injecting syringe. Constant voltage was applied to the sensors, and current was measured by digital picoammeter. Air was allowed to pass into the glass dome after every gas exposure cycle.

The TG curve in Figure 1 shows a minor weight loss step (20%) between 30°C and 270°C, as well as two major weight loss steps (60%) in between 270°C and 455°C. No further weight loss was observed beyond 455°C and up to 1000°C. The minor weight loss in the as-spun $MgFe_2O_4$ nanopowder was due to loss of moisture by trapped solvent like water and existing carbon dioxide during the combustion, whereas the major weight loss was due to the combustion of organic matrix. On the DTA curve, main exothermic peaks were observed at ~ 290°C and ~ 450°C, suggesting that the thermal events were related to the decomposition of Mg and Fe nitrates carried out by dehydration of the nanopowder, which was confirmed by a drastic weight loss in TG curve at the corresponding temperature range (270–455°C). The plateau formed

between 455°C and 1000°C on the TG curve indicates the formation of crystalline $MgFe_2O_4$, which acts as the decomposition product after combustion reaction. This was confirmed by XRD and FTIR analysis. Synthesis of $MgFe_2O_4$ was carried out by combustion reaction represented by the following equations.

$$2C_2NH_3O_2 + (9/2)O_2 \rightarrow N_2\uparrow + 4CO_2\uparrow + 5H_2O\uparrow, \quad (1)$$

$$Mg(NO_3)_3 + Fe(NO_3)_3 + 4C_2H_5NO_2 \rightarrow MgFe_2O_4 + 8CO_2\uparrow + 10H_2O\uparrow + 5N_2\uparrow. \quad (2)$$

The XRD patterns of the calcined $MgFe_2O_4$ are shown in Figure 2. All of the observed main peaks were indexed and matched with the spinel $MgFe_2O_4$ in the standard data (JCPD No. 88-1935). The average crystallite sizes of $MgFe_2O_4$ sample were calculated X-ray line broadening reflections of the $MgFe_2O_4$ sample were (220), (311), (400), (511) and (440) calculated using Scherrer's equation (i.e. $D = 0.89k/(\beta \cos \theta)$, where $k$ is the wavelength

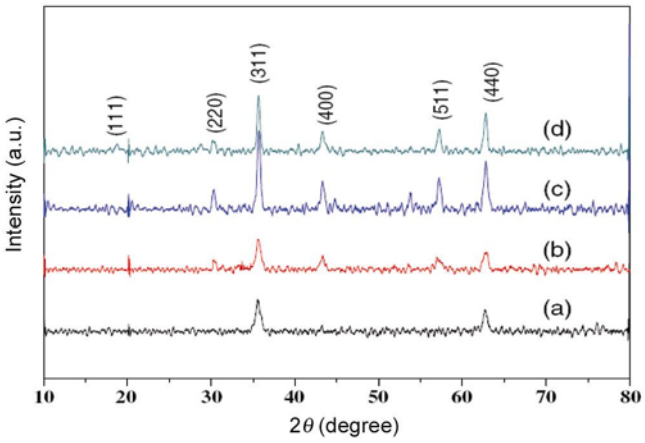


**Figure 2.** XRD pattern of calcined mixed precursor $MgFe_2O_4$ in air to: (a) 500°C, (b) 600°C, (c) 700°C and (d) 800°C.

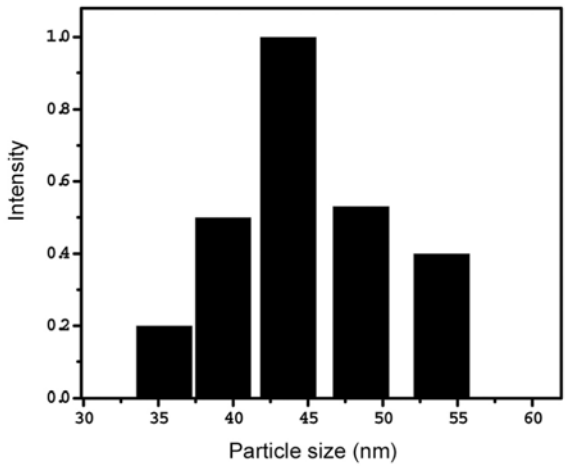


**Figure 3.** Particle size distribution studies.

of the X-ray, $K$ is a constant taken as 0.89, $h$ the diffraction angle, and $b$ is the full width at half-maximum[31–34], and were found to be 16, 18, 25 and 26 nm for the $MgFe_2O_4$ samples calcined at 500°C, 600°C, 700°C and 800°C respectively.

Particle size distribution studies were carried out using dynamic light scattering techniques (Figure 3; DLS via laser input energy at 632 nm). It was observed that magnesium iron oxide nanoparticles were narrow in size and was distributed within the range of 30–55 nm, which matched well with the calculated value using Scherrer equation.

The detailed morphology and crystalline structure of two $MgFe_2O_4$ samples, calcined at 600°C for 4 h were further studied using TEM. The TEM bright-field images with corresponding selected-area electron diffraction (SAED) patterns of the samples are shown in Figure 4. From the TEM bright field images, it is clearly seen that the samples consist of packed $MgFe_2O_4$ crystallite particles of ~25–80 nm diameter. The particle size of $MgFe_2O_4$ was seen to be uniform.

Figure 5 depicts the *I–V* characteristics of *E. coli* as micron particles and nanoparticle $MgFe_2O_4$ films. From the symmetrical *I–V* characteristics, it is clear that the silver contacts on the films are ohmic in nature.

Figure 6 shows the variation of log (conductivity) with temperature. The conductivity values of the sample increase with operating temperature. The increase in conductivity with increasing temperature could be attributed to negative temperature coefficient of resistance and semiconducting nature of *E. coli* and $MgFe_2O_4$ thick film. It can be observed from the figure that the electrical conductivity of *E. coli* and $MgFe_2O_4$ film was nearly linear in the temperature range from 30°C to 40°C in ambient air.

Gas response ($S$) is defined as the ratio of the change in conductance of the sensor on exposure to the target gas with the original conductance in air. The comparative relation for $S$ is:

$$S = \frac{G_g - G_a}{G_a},$$

where $G_a$ and $G_g$ are the conductance of the sensor in air and in the target gas medium respectively.

Selectivity or specificity is defined as the maximum ability of a sensor to respond to ammonia gas followed by other gases. The time taken for the sensors to attain 90% of the original conductance is the recovery time.

Table 1 and Figure 7 depict the variation in response of *E. coli* to $NH_3$ (at 1000 ppm) under various operating temperatures. The largest response of prepared *E. coli* and $MgFe_2O_4$ thick film was observed to be 6.70° at 37°C. The ammonia response at 37°C temperature was expected to be monitored by adsorption of moisture on the *E. coli*–$MgFe_2O_4$ film. The cumulative effect would decrease the resistance of the film, giving a response to ammonia gas

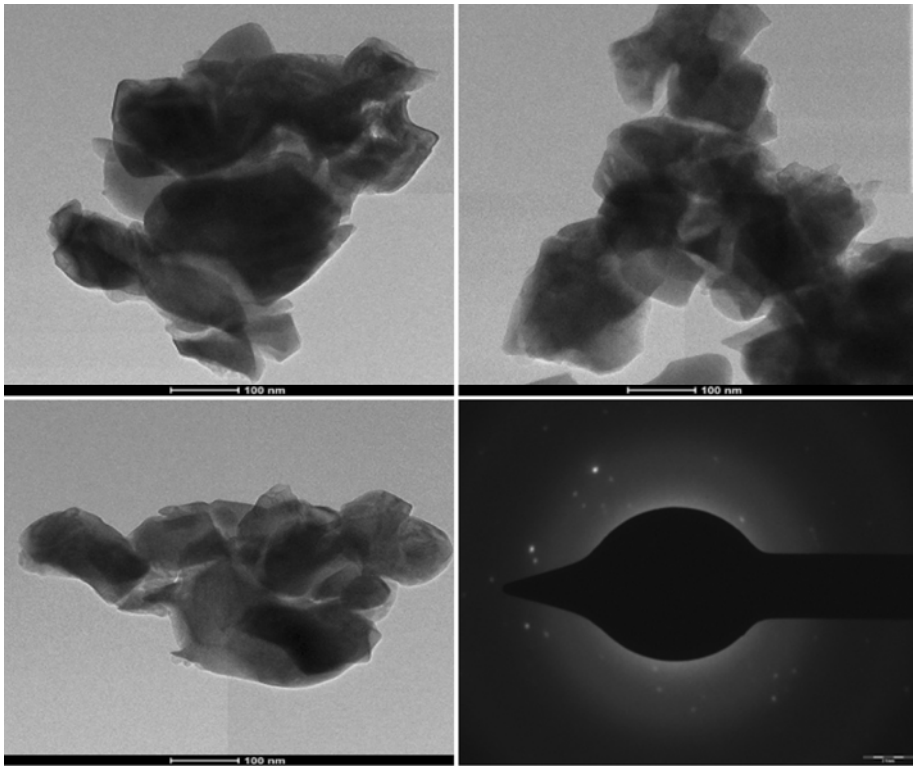


**Figure 4.** TEM images with corresponding SAED patterns of the $MgFe_2O_4$ samples calcined in air for 4 h at 600°C.

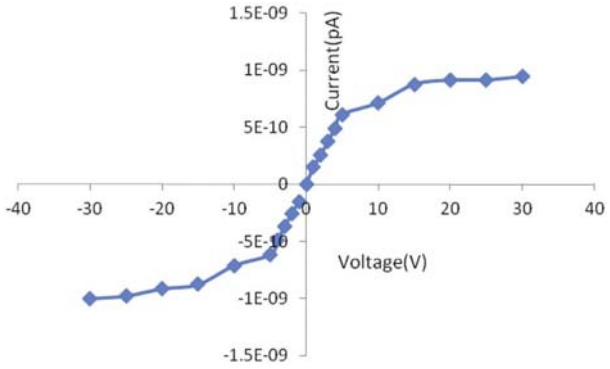


**Figure 5.** *I–V* characteristics of the sensor.

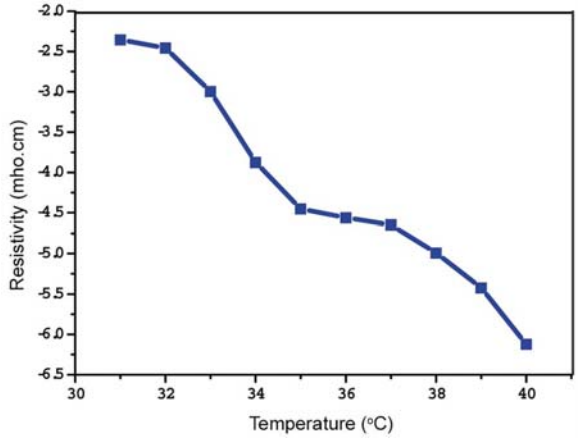


**Figure 6.** Resistivity variation of *Escherichia coli* $MgFe_2O_4$ thick film with reciprocal operating temperatures.

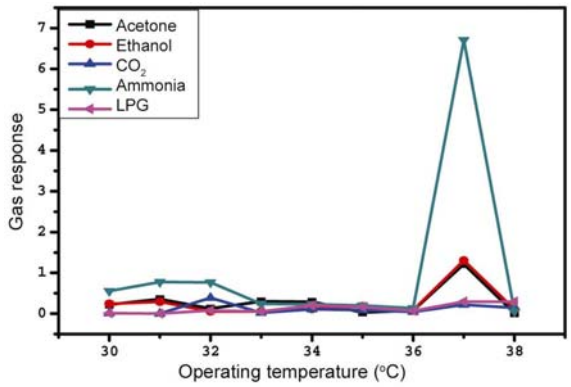


**Figure 7.** Variation in gas response of *E. coli*–$MgFe_2O_4$ thick film under different operating temperatures.

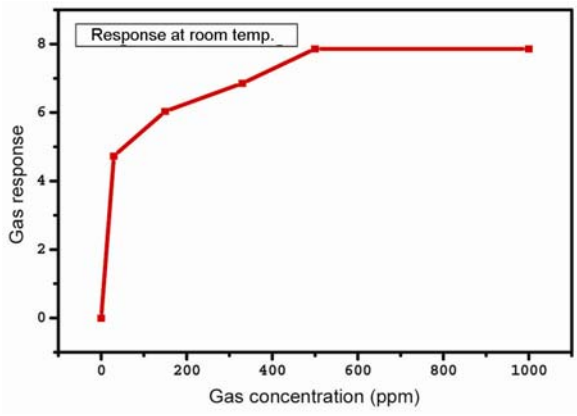


**Figure 8.** Variation of gas response with gas concentration.

**Table 1.** Variation in gas response of *Escherichia coli* $MgFe_2O_4$ thick film with different operating temperatures

| Temperature (°C) | Acetone (ppm) | Ethanol (ppm) | $CO_2$ (ppm) | $NH_3$ (ppm) | LPG (ppm) |
|---|---|---|---|---|---|
| 38 | 0.01 | 0.1052 | 0.1428 | 0.0555 | 0.29411 |
| 37 | 1.213 | 1.302 | 0.21818 | 6.7065 | 0.2951 |
| 36 | 0.0746 | 0.08823 | 0.04412 | 0.13285 | 0.06493 |
| 35 | 0.0304 | 0.17931 | 0.08695 | 0.2 | 0.16 |
| 34 | 0.2875 | 0.11428 | 0.1111 | 0.2337 | 0.2058 |
| 33 | 0.2958 | 0.05408 | 0.0204 | 0.2437 | 0.05194 |
| 32 | 0.123 | 0.05405 | 0.3896 | 0.7647 | 0.07812 |
| 31 | 0.355 | 0.29082 | 0.0012 | 0.7747 | 1.00 |
| 30 | 0.221 | 0.24 | 0.012 | 0.553 | 0.01 |

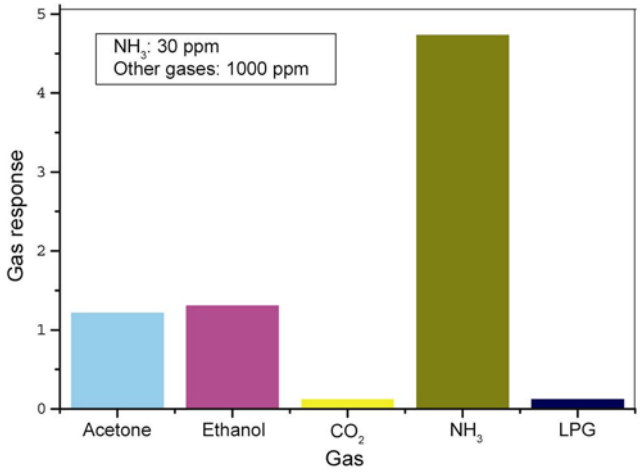


**Figure 9.** Selectivity of *E. coli*–$MgFe_2O_4$ thick film among various gases.

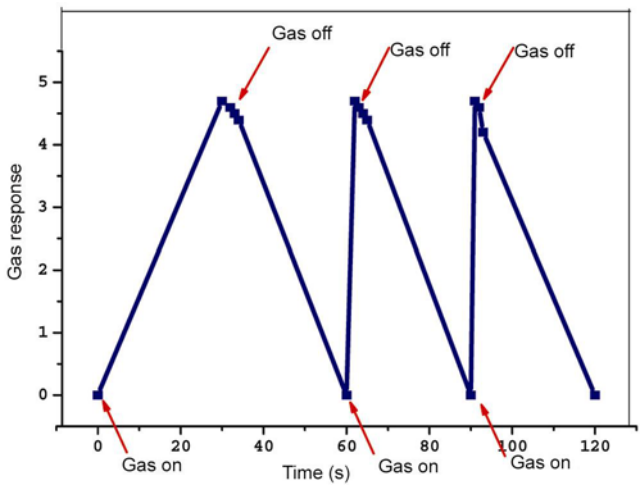


**Figure 10.** Response and recovery of the sensors.

at 37°C. Except 37°C, no more oxygen adsorption was observed. Therefore, the oxygen adsorption–desorption mechanism is employed at 37°C to sense $NH_3$ and not at other temperatures.

The variation in gas response of *E. coli*–$MgFe_2O_4$ sample with $NH_3$ gas concentration at 37°C is represented in Figure 8. This film was exposed to varying concentrations of $NH_3$ gas. For thick film of *E. coli*–$MgFe_2O_4$, the response increases continuously with increasing gas concentration up to 30 ppm at 37°C. The increasing rate of response was relatively more up to 30 ppm, but smaller between 30 and 1000 ppm. Thus, the active region of the sensors was to be found up to 30 ppm. At lower gas concentration, the unimolecular layer of gas molecules was formed on the surface of the sensor, which can further interact giving rise to larger response.

Figure 9 depicts the selectivity of the *E. coli*–$MgFe_2O_4$ sensor for $NH_3$ gas (30 ppm) at 37°C. The sensor shows high selectivity to $NH_3$ at 30 ppm and 37°C temperature, unlike other gases like ethanol, acetone, LPG and $CO_2$ which showed high selectivity at 1000 ppm.

Figure 10 depicts the response and recovery of the *E. coli*–$MgFe_2O_4$ sensor. The response was quick for $NH_3$ (~ 15 s) at 30 ppm, while the recovery was considerably fast (~ 60 s).

The *E. coli*–$MgFe_2O_4$ thick film causes the formation of inter-grain boundaries of *E. coli*–$MgFe_2O_4$–*E. coli*–$MgFe_2O_4$ grains. The exposed gases molecule capture the lattice oxygen from the surface of the film at various temperatures. This would result in oxygen deficiency in the bulk of the material, preferably at the surface. The semiconductivity in *E. coli*–$MgFe_2O_4$ may be due to large oxygen deficiency. The increase in the conductivity of *E. coli*–$MgFe_2O_4$ thick film could be attributed to the charge-carrier generation mechanism resulting from the electronic changes in *E. coli*–$MgFe_2O_4$ thick film of the applied grains to generate the electrons. These generated electrons and the donor levels formed in the energy band gap of *E. coli*–$MgFe_2O_4$ will contribute to increase in conductivity. This results in increasing the conductance of the film at various temperatures. During the reaction the catalyst $MgFe_2O_4$ continuously supports *E. coli*. This is required to obtain optimum result.

The nanostructured $MgFe_2O_4$ alone acts as sensor for ammonia gas, while *E. coli*'s unit is in micron, therefore

particle shows comparatively low results for ammonia. Hence applied *E. coli*–$MgFe_2O_4$, $MgFe_2O_4$ act as catalyst for *E. coli*. *E. coli* itself has its own ability to detect the gas and sense, but it is new target to search out the exact mechanisms. It is under process.

In conclusion, the *E. coli*–$MgFe_2O_4$ synthesis route employed in this study may also be used for the synthesis of other bacterial cells and metal oxides respectively. These applied nanoparticles show good *I–V* characteristics with ideal semiconducting property. Among all additives tested, *E. coli*–$MgFe_2O_4$ the ammonia gas showed highest response to ammonia at 37°C. The applied sensor showed rapid response and fast recovery to ammonia gas. The sensor has good selectivity to ammonia compared to ethanol, acetone, $CO_2$ and LPG.


1. Blattner, F. R. *et al.*, The complete genome sequence of *Escherichia coli* K-12. *Science*, 1997, **277**, 1453–1462.
2. Sugimoto, M., The past, present and future of ferrites. *J. Am. Ceram. Soc.*, 1999, **82**, 269–280.
3. Liu, Y., Liu, Z. M., Yang, Y., Yang, H. F., Shen, G. L. and Yu, R. Q., *Sensors Actuators B*, 2005, **107**, 600–604.
4. Hankare, P. P., Jadhav, S. D., Sankpal, U. B., Patil, R. P., Sasikala, R. and Mulla, I. S., Gas sensing properties of magnesium ferrite prepared by co-precipitation method. *J. Alloys Compd.*, 2009, **488**, 270–272.
5. Willey, R. J., Noirclerc, P. and Busca, G., *Chem. Eng. Commun*., 1993, **35**, 123.
6. Oliver, S. A., Willey, R. J., Hamdeh, H. H., Oliveri, G. and Busca, G., FT-IR spectra of the $MgFe_2O_4$ composite samples calcined in air. *Scr. Mater*., 1995, **33**, 1695.
7. Wu, W., He, Q. and Jiang, C., Magnetic iron oxide nanoparticles: synthesis and surface functionalization strategies. *Nanoscale Res. Lett.*, 2008, **3**, 397.
8. Hua, Z. H., Chen, R. S., Li, C. L., Yang, S. G., Lu, M., Gu, X. B. and Du, Y. W., *J. Alloys Compd*., 2007, **427**, 199.
9. Corr, S. A., Rakovich, Y. P. and Gun'ko, Y. K., Magnetic iron oxide nanoparticles: synthesis and surface functionalization strategies. *Nanoscale Res. Lett*., 2008, **3**, 87.
10. Lai, Z., Xu, G. and Zheng, Y., Microwave assisted low temperature synthesis of MnZn ferrite nanoparticles. *Nanoscale Res. Lett*., 2007, **2**, 40.
11. Bangale, S. V., Patil, D. R. and Bamane, S. R., Nanostructured spinel $ZnFe_2O_4$ for the detection of chlorine gas. *Sensors Transducers*, 2011, **134**, 107–119.
12. Xinshu, N., Yanli, L. and Jiaqiang, X., *Chin. Funct. Mater*., 2002, **33**, 413.
13. Satyanarayana, L., Madhusudan, K., Reddy, V. M. and Sunkara, *Mater. Chem. Phys*., 2003, **82**, 21.
14. Liu, C., Zou, B., Rondinone, A. J. and Zhang, Z. J., Atomic level magnetic coupling. *J. Am. Chem. Soc*., 2000, **122**, 6263.
15. Busca, G., Finocchio, E., Lorenzelli, V., Trombetta, M. and Rossini, S. A., IR study of alkene allylic activation on magnesium ferrite and alumina catalysts. *J. Chem. Soc. Faraday Trans*., 1996, **92**, 4687.
16. Shimizu, Y., Arai, H. and Seiyama, T., Theoretical studies on the impedance humidity characteristic of ceramic humidity sensors. *Sens. Actuators B*, 1985, **7**, 11–22.
17. Benko, F. A. and Koffyberg, F. P., Arrhenius plots of dc electrical conductivity of the as-deposited $CuCr_2$ film. *Mater. Res. Bull*., 1986, **21**, 1183.
18. Sugimoto, M., The past, present and future of ferrites. *J. Am. Ceram. Soc*., 1999, **82**, 269–280.
19. Kamble, R. B. and Mathe, V. L., Nanocrystalline nickel ferrite thick films as an. *Sensors Actuatora B*, 2008, **131**, 205–209.
20. McMichael, R. D., Shull, R. D., Swartzendruber, L. J., Bennett, L. H. and Watson, R. E., Magnetocaloric effect in superparamagnets. *J. Magn. Magn. Mater*., 1992, **11**, 29–33.
21. Gopal Reddy, C. V., Manorama, S. V. and Rao, V. J., Preparation and characterization of ferrites as gas sensor materials. *J. Mater. Sci. Lett*., 2000, **9**, 775–778.
22. Chen, N. S., Yang, X. J., Liu, E. S. and Huang, J. L., Reducing gas-sensing properties of ferrite compounds $MFe_2O_4$ (M = Cu, Zn, Cd, Mg). *Sensors Actuators B*, 2000, **66**, 178180.
23. Rezlescu, N., Rezlescu, E. and Popa, P. D., Gas sensitivity of nanocrystalline nickel ferrite. *J. Optoelectron.. Adv. Mater.*, 2006, **8**, 1016.
24. Khetre, S. M., Jadhav, H. V., Jagdale, P. N., Bangale, S. V. and Bamane, S. R., Use of mixed metal oxide as a catalyst in the decomposition of hydrogen peroxide. *Adv. Appl. Sci. Res.*, 2011, **2**, 252–259.
25. Kodama, T., Wada, Y., Yamamoto, T. and Tsuji, M., Synthesis and characterization of ultrafine nickel(II)-bearing ferrites ($Ni_xFe_{3-x}O_4$, $x$ = 0.14–1.0)M. *J. Mater. Chem*., 1995, **5**, 1413.
26. Hirano, S., Yogo, T., Kikuta, K., Asai, E., Sugiyama, K. and Yamamoto, H., Preparation and phase separation behavior of cobalt iron oxide film. *J. Am. Ceram. Soc*., 1993, **76**, 1788.
27. Hochepied, J.-F., Bonville, P. and Pileni, M. P., Nonstoichiometric zinc ferrite nanocrystals: syntheses and unusual magnetic properties. *J. Phys. Chem. B*, 2000, **104**, 905–912.
28. Bangale, S. V. and Bamane, S. R., Preparation and electrical properties of nanostructured spinel $ZnCr_2O_4$ by combustion route. *J. Mater. Sci.: Mater. Electron*, 2013, **24**, 277–281.
29. Verma, S., Joy, P. A., Khollam, Y. B., Potdar, H. S. and Deshpande, S. B., Synthesis of nanosized $MgFe_2O_4$ powders by microwave hydrothermal method. *Mater. Lett*., 2004, **58**, 1092.
30. Bangale, S. V., Khetre, S. M. and Bamane, S. R., Synthesis, characterization and hydrophilic properties of nanocrystalline $ZnCo_2O_4$ oxide by combustion route. *Der Chem. Sin.*, 2011, **2**, 303–311.
31. Cullity, B. D. and Stock, S. R., *Elements of X-ray Diffraction*, Prentice Hall, NJ, 2001, 3rd end.
32. Hongshui Wang, Xueliang Qiao, Jianguo Chen, Xiaojian Wang[a], Shiyuan Ding, Mechanisms of PVP in the preparation of silver nanoparticles. *Mater. Chem. Phys*., 2005, **94**, 449–453.
33. Pradeep, A. and Chandrasekaran, G., Magnesium, FTIR study of Ni, Cu and Zn substituted nano-particles of $MgFe_2O_4$. *Mater. Lett*., 2006, **60**, 371.
34. Rao, G. V. S., Rao, C. N. R. and Ferraro, J. R., Infrared and electronic spectra of rare earth perovskites: ortho-chromites, -manganites and -ferrites. *Appl. Spectrosc*., 1970, **24**, 436–445.


ACKNOWLEDGEMENT. S.V.B. thanks IIT Bombay for providing TEM analysis and S.B. thank N. G. Vedak and N. S. Yadav for providing necessary facilities and encouragement during research work.

Received 18 November 2011; revised accepted 16 August 2013